



A new method on the limit cycle stability analysis of digitally controlled interleaved DC–DC converters[☆]

George Gkizas^{*}, Damian Giaouris, Volker Pickert

School of Electrical and Electronic Engineering, Newcastle University, Newcastle Upon Tyne, NE1 7RU, United Kingdom



ARTICLE INFO

Keywords:

Interleaved boost converter
Digital control
Limit cycle stability
Monodromy matrix
State feedback

ABSTRACT

Nowadays, the requirement to ameliorate efficiency in power conversion systems along with the demand for increased power rating gives rise to the implementation of interleaving operation. Interleaving in conjunction with digital state feedback control provide the ability to create sophisticated control schemes which allow for high efficiency under a wide range of operating conditions and restrictions. Along these lines, the interleaved boost converter finds widespread application in a variety of cases such as battery charging, renewable energy sources and distributed power systems. A very salient aspect concerning the performance of the converter is the occurrence of limit cycle instabilities that can have an adverse effect on the operation of the converter resulting in efficiency and lifetime reduction. These instabilities are a trait of the piecewise linear nature of the system dynamics, in which case, a bifurcation analysis is required to investigate their influence on the system. However, in the case of interleaving along with digital control the standard implementation of the bifurcation analysis for determining the Monodromy matrix is impeded by the dependency of the system of past sampled states. As a consequence, the conventional approaches found in literature are inadequate when it comes to predicting and avoiding these kind of instabilities. This paper addresses the specific issues and presents a novel approach on defining the Monodromy Matrix and deciding upon the stability of the limit cycle. The proposed approach relieves the dependence of the system on past samples by augmenting the first return map with expressions that describe the evolution of the control laws. The interleaved boost converter is used as a case study. Finally, numerical, analytical and experimental results validate our work.

1. Introduction

In recent years interleaved converters have been in the spotlight of research and investigation due to their advantages over other simple topologies. Several interleaved converter topologies have been proposed and are implemented in a wide range of applications. These include electric vehicles and battery charging (Jung, Lempidis, Holsch, & Steffen, 2015a; Jung, Lempidis, Holsch, & Steffen, 2015b; Wang & Khaligh, 2015), the exploitation of renewable energy sources like photovoltaic-cells and fuel-cells (Mouli, Schijffelen, Bauer, & Zeman, 2017; Pulvirenti et al., 2013; Shojaeian, Heydari, & Hasanzadeh, 2017). A common characteristic among these applications is the important role of a high efficiency which is the main reason why interleaving constitutes an appealing technique. Interleaving in conjunction with multilevel topologies provides the ability to increase efficiency and the power rating of the system due the introduction of extra phases. The load is distributed among the phases which allows the relief of stress on the switching components, power losses on the system are mitigated and current and voltage ripples are diminished as well. In this

regard, the efficiency is substantially elevated (Choi, Jang, Ciobotaru, & Agelidis, 2016; Michal, 2016; Tseng & Huang, 2014). In this work the interleaved boost converter was chosen as a case study since it constitutes a ubiquitous converter among the different topologies.

State of the art circuits employ digital control schemes due to their advantages such as low power, immunity to analog component variations and the potential for more sophisticated control schemes (Erickson & Maksimovic, 2001). Several digital control schemes have been proposed for compensating the interleaved boost converter including online self-tuning control (Elsied et al., 2016), fault-tolerant control for renewable energy systems (Guilbert, Gaillard, N'Diaye and Djerdir, 2016; Guilbert, N'Diaye, Gaillard and Djerdir, 2016), adaptive control (Salhi, Ahmed-Ali, Fadil, Magarotto, & Giri, 2013; Zhang, Xu, & Liu, 2014) and more advanced control schemes like model predictive control (Karamanakos, Geyer, & Manias, 2013; König, Gregorčič, & Jakubek, 2013).

A crucial aspect of the boost converter topologies are their innate nonlinear dynamics. A control design that does not take them into account can drive the converter to undesirable operational regimes

[☆] This paper was not presented at any IFAC meeting.

^{*} Corresponding author.

E-mail addresses: g.gkizas2@ncl.ac.uk (G. Gkizas), damian.giaouris@newcastle.ac.uk (D. Giaouris), volker.pickert@newcastle.ac.uk (V. Pickert).

as it is illustrated in Gkizas et al. (2016, 2018). However, there has been research to some extent on tackling the nonlinear behaviour of the interleaved boost converter with the employment of methods like passivity-base control (Cisneros et al., 2015), nonlinear adaptive control (Fadil, Giri, Guerrero, Haloua, & Abouloifa, 2011), nonlinear sliding mode control (Giral, Martinez-Salamero, Leyva, & Maixe, 2000; Saadi et al., 2016) and constrained stabilization (Gkizas et al., 2016, 2018; Yfoulis et al., 2014, 2015).

As it can be deduced the interleaved boost converter constitutes a system that instigates several challenges that need to be dealt since it pertains to a wide range of applications, evident by the preceding statements. Furthermore, a common characteristic of the aforementioned approaches to the investigation, and consequently the control, of the interleaved boost converter is that they mostly consider the bilinear dynamics without taking into account the underlying switching action due to the utilization of averaging (Erickson & Maksimovic, 2001). Averaging is a common practice since the piecewise linear dynamical description of the system is simplified by excluding the switching dynamics and, thus, rendering it amenable to control theory. However, the switching action can give rise to bifurcation phenomena so that fast-scale, slow-scale and saddle-node instabilities may emerge. At this point it should be mentioned, in the case of the interleaved boost converter, that certain saddle-node bifurcations can be foreseen by the average model, due to the inherent bilinear dynamics (Gkizas et al., 2016), however the remainder need to be investigated by studying the stability of the non-smooth limit cycle of the piecewise linear system. The significance of conducting such an analysis is that these kind of instabilities can greatly affect the operation of the system by increasing voltage and current ripples, attributed to fast-scale instabilities (Banerjee & Verghese, 2001; Giaouris, Banerjee, Zahawi, & Pickert, 2008), and superimpose a low frequency high amplitude harmonic, a trait of slow-scale instabilities (Aroudi, Benadero, Toribio, & Olivar, 1999; Zhusubaliyev, Mosekilde, & Yanochkina, 2011), which will cause a drop in efficiency and also cause problems concerning controller saturation. Evidently, a bifurcation analysis is rendered as a necessity. Along these lines, there have been studies on the limit cycle stability of the interleaved boost converter (Giaouris et al., 2014; Wu, Pickert, & Giaouris, 2014; Wu, Pickert, Giaouris, & Ji, 2017), however, the lack of research whilst under the framework of digital compensation is noticeable.

The means of investigating the limit cycle stability of piecewise smooth dynamical systems are based on accurate approaches which can entail discrete-time mappings (di Bernardo & Vasca, 2000). The stability analysis of periodic solution of differential equation with discontinuous right-hand sides was first proposed in Aizerman and Gantmakher (1958). Filippov (1988) provides the saltation matrix that facilitates the investigation of stability of these orbits (Aroudi, Iu, & Hiskens, 2015; Banerjee & Verghese, 2001). Other proficient approaches on the investigation of stability have been reported in literature Baushev, Zhusubaliyev, Kolokolov, and Terekhin (1992), Zhusubaliyev, Soukhoterina, Rudakov, Kolokolov and Mosekilde (2001) and Zhusubaliyev, Soukhoterina, and Mosekilde (2003). The common ground shared amongst them is the underlying idea with which the stability is studied. The foundation of this idea is the introduction of a perturbation and the monitoring of its evolution in the span of one clock period.

Albeit the fact that the aforementioned ideas have been successfully implemented in many cases they, unfortunately, fall short when it comes to interleaving under digital control. The reason is that the processes of applying these methods in this particular case are impeded due to the dependence of the limit cycle on past sampled states. In simple terms, certain important aspects during the process of the bifurcation analysis cannot be cast explicitly due to this dependence. This paper provides the solution to this impediment and the requisite method for conducting the bifurcation analysis. As it will be shown the first return map of the system is expressed in such a way that it is relieved from the dependence on the past sampled state vector. As a consequence,

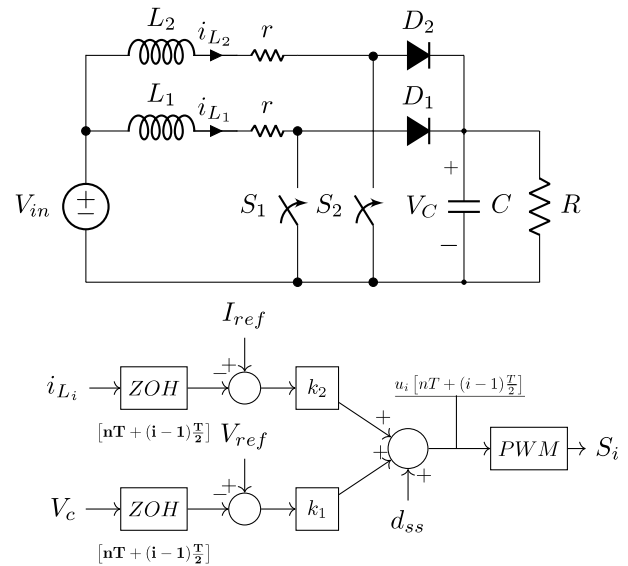


Fig. 1. Two-legged interleaved DC-DC boost converter with state feedback controller.

another very important contribution of this analysis, is the insight that comes along with the proposed method. Evidently, it is shown that the method is applicable in the case where delays are introduced, due to physical restrictions, by experimentally implementing the digital control law. To this end, the experimentation carried out in this work successfully corroborates the above assertion.

The paper is organized as follows: The description of the system, along with the mathematical modelling, takes place in Section 2. The bifurcation behaviour of the system under static state-feedback control is presented in Section 3 and the bifurcation analysis is conducted in Section 4. Moreover, in Section 5 a dynamic state-feedback controller and its implications on the limit cycle stability are considered. Section 6 unravels and deals with implication on the limit cycle stability stemming from the physical implementation of the control laws. The experimental results are presented in Section 7. This work concludes in Section 8.

2. System description

The system under consideration is a two-phase interleaved boost converter compensated by digital static state feedback control. State feedback control is chosen because it constitutes a control scheme that offers many advantages over other conventional control methods, e.g. PI, PID or Cascade control. Apart from the established facts that it relieves them system of the introduction of additional poles and zeros, which would otherwise increase complexity and overshoot at transients respectively, it is also amenable to optimal and robust control frameworks (Geyer, Papafotiou, & Morari, 2008). Furthermore, the boost converter topologies exhibit a non-minimum phase behaviour that complicates their control even further. State feedback overcomes these obstacles. The two-legged interleaved boost converter along with the component values are given in Fig. 1 and Table 1 respectively.

The implementation of interleaving dictates a phase difference of $2\pi/N$ for every PWM modulator relative to each leg, with N being the number of legs. Moreover, the state-feedback controllers, for driving each switch, are constructed by taking advantage of the symmetry of the system and utilizing only two states for the realization of each individual controller. Namely, the state feedback control law for each switch is realized by making use of the capacitor voltage and the corresponding current that the switch is manipulating, as described by (1) and (2). This method has been extensively analysed by the author in Gkizas et al. (2016, 2018). Based on that analysis the static state

Table 1
Interleaved boost converter parameter values.

Parameter	Value
R	40 Ω
V_{in}	5 V
L	1 mH
C	20 μF
r	0.1 Ω
N	2

feedback gains that will provide the system with a damping factor $\zeta = 0.7$ and damped natural frequency $\omega_d = 2000r/s$ are $k_1 = -0.0424$ and $k_2 = 0.1595$.

$$u_1[nT] = -k_1(x_1[nT] - V_{ref}) - k_2(x_2[nT] - I_{ref}) + d_{ss} \quad (1)$$

$$u_2 \left[nT + \frac{T}{2} \right] = -k_1 \left(x_1 \left[nT + \frac{T}{2} \right] - V_{ref} \right) - k_2 \left(x_3 \left[nT + \frac{T}{2} \right] - I_{ref} \right) + d_{ss} \quad (2)$$

2.1. Mathematical modelling

The dynamics that govern the two-legged converter can be described by the piecewise linear system of differential equation in (3) where the corresponding matrices are given in (4). In the aforementioned equations the state vector is represented by $\mathbf{x}(t) = [x_1(t) \ x_2(t) \ x_3(t)]^T$, where $t \in \mathbb{R}$, $\mathbf{x}(t) \in \mathbb{R}^n$, $\mathbf{A}_1, \mathbf{A}_2, \mathbf{A}_3, \mathbf{A}_4 \in \mathbb{R}^{n \times n}$ and $\mathbf{B} \in \mathbb{R}^{n \times 1}$, with $n = 3$. State $x_1(t)$ represents the capacitor voltage and states $x_2(t)$ and $x_3(t)$ the currents of inductors L_1 and L_2 respectively. The states of the switches denoted as ON and OFF in (3) correspond to a switch conducting or being open respectively.

$$\dot{\mathbf{x}}(t) = \begin{cases} \mathbf{A}_1 \mathbf{x}(t) + \mathbf{B} V_{in} & S_1 = ON \quad S_2 = ON \\ \mathbf{A}_2 \mathbf{x}(t) + \mathbf{B} V_{in} & S_1 = OFF \quad S_2 = ON \\ \mathbf{A}_3 \mathbf{x}(t) + \mathbf{B} V_{in} & S_1 = ON \quad S_2 = OFF \\ \mathbf{A}_4 \mathbf{x}(t) + \mathbf{B} V_{in} & S_1 = OFF \quad S_2 = OFF \end{cases} \quad (3)$$

$$\mathbf{A}_1 = \begin{bmatrix} -\frac{1}{RC} & 0 & 0 \\ 0 & -\frac{r}{L} & 0 \\ 0 & 0 & -\frac{r}{L} \end{bmatrix} \quad \mathbf{A}_4 = \begin{bmatrix} -\frac{1}{RC} & \frac{1}{C} & \frac{1}{C} \\ -\frac{1}{L} & -\frac{r}{L} & 0 \\ -\frac{1}{L} & 0 & -\frac{r}{L} \end{bmatrix} \quad (4)$$

$$\mathbf{A}_3 = \begin{bmatrix} -\frac{1}{RC} & 0 & \frac{1}{C} \\ 0 & -\frac{r}{L} & 0 \\ -\frac{1}{L} & 0 & -\frac{r}{L} \end{bmatrix} \quad \mathbf{A}_2 = \begin{bmatrix} -\frac{1}{RC} & \frac{1}{C} & 0 \\ -\frac{1}{L} & -\frac{r}{L} & 0 \\ 0 & 0 & -\frac{r}{L} \end{bmatrix}$$

$$\mathbf{B} = [0 \ 1/L \ 1/L]^T$$

3. Bifurcation behaviour of the system

The set of gains chosen after a pole placement technique may meet the performance criteria at the equilibrium point, however due to the bilinear nature of the system, they also give rise to other equilibrium points that are comprised of another stable and saddle fixed point. This is typical behaviour of a boost converter and depending on the position of the fixed point in state space the intensity of the non-linear phenomena may be different (Giaouris, Yfoulis, Voutetakis, & Papadopoulou, 2013). In order to capture a situation that provides a plethora of interesting dynamical phenomena, that will facilitate the

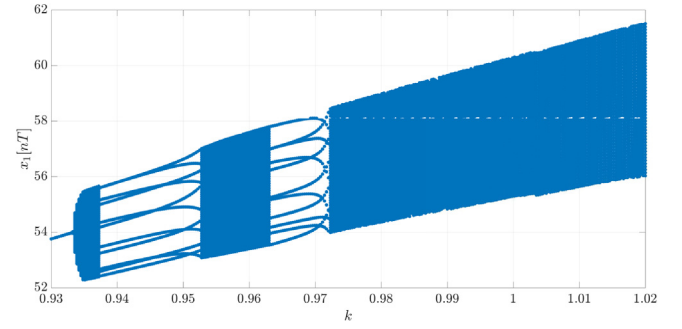


Fig. 2. Bifurcation diagram for $k \in [0.93 \ 1.02]$.

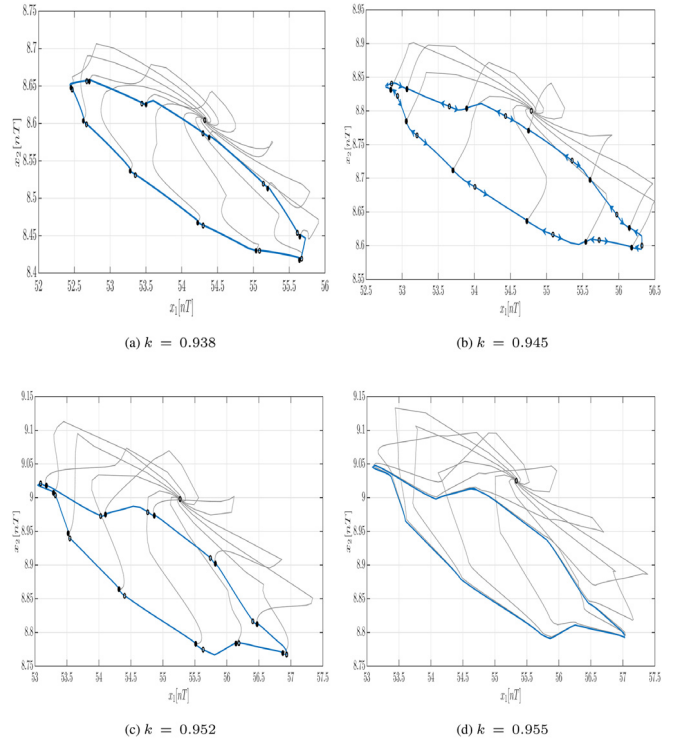


Fig. 3. Period-11 orbits. The solid black dots and the hollow black dots represent the stable and unstable periodic orbits respectively.

validation of proposed method in this work, a fixed point that lays far away from the origin is taken under consideration.

The bifurcation parameter chosen to be varied at the aforementioned fixed point is gain k_1 which corresponds the static state feedback control law in (1). This is denoted by $k_1 = -0.0424 \cdot k$, where $k \in \mathbb{R}_+$. The bifurcation diagram given in Fig. 2 depicts the bifurcation behaviour of the system around the fixed point under consideration. For $k = 0.934$ a smooth Neimark–Sacker bifurcation takes place that gives rise to a torus in state space. At approximately $k = 0.938$ a stable and an unstable period-11 is created as depicted in Fig. 3a. The period-11 orbits vanish at approximately $k = 0.952$, Fig. 3c, due to the collision of the stable and unstable fixed points. The process that is portrayed in Fig. 3 is repeated for $k \in [0.963 \ 0.972]$.

The occurrence and analysis of the intricate phenomena portrayed in Figs. 2 and 3 will be the subject of the subsequent section.

4. Bifurcation analysis

The aim of this section is to conduct the bifurcation analysis and provide the methods to identify the instabilities that occur with respect

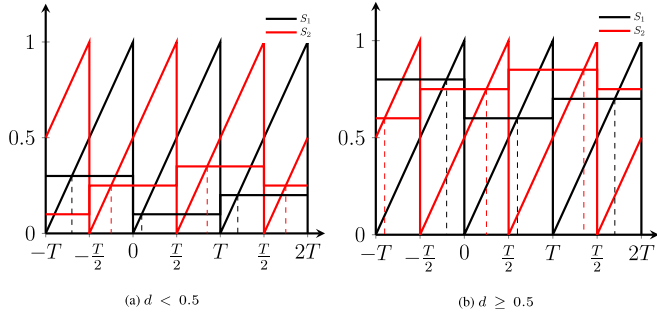


Fig. 4. PWM type 1 operation of the converter. (For interpretation of the references to colour in this figure legend, the reader is referred to the web version of this article.)

Table 2

Changes and duration of operation in topologies for the two different cases where $d \geq 0.5$ and $d < 0.5$ in a switching cycle T . Notations S_1, S_2 and \bar{S}_1, \bar{S}_2 represent the OFF and ON state of the switches respectively.

$d \geq 0.5$				
Sequence	$S_1 S_2$	$S_1 \bar{S}_2$	$\bar{S}_1 S_2$	$\bar{S}_1 \bar{S}_2$
Duration	$(d - 0.5)T$			
$d < 0.5$				
Sequence	$S_1 \bar{S}_2$	$\bar{S}_1 \bar{S}_2$	$\bar{S}_1 S_2$	$S_1 \bar{S}_2$
Duration	dT		$(0.5 - d)T$	

to the variation of the bifurcation parameter, i.e. parameter k . The first step that needs to be taken is the identification of the fixed points for both the period-1 and period-11 orbits. Then appropriate first return maps will be derived that will describe the evolution of the state vector in a limit cycle. Eventually their stability will be studied by deriving the Jacobians of first return maps and carrying out an eigen-decomposition.

Another important aspect of the operation of the converter is that the sequence of topological changes depends on the values of duty cycles being below or above 0.5. To illustrate this concept we refer to Fig. 4. In both Figs. 4a and 4b the red sawtooth trace, that represents the carrier signal of the second phase, has a phase shift of $T/2$ seconds with respect to the black trace, corresponding to the carrier signal of the first phase. The control law in both cases is formed every nT and $nT + T/2$ for the first and second phase respectively. Moreover, in both cases the control signal is kept constant for the span of T seconds. This is the basic principle behind the digital implementation of interleaving. One can discern that in Fig. 4a the sequence of topological changes, or alternatively the sequence of states that the switches assume, in every cycle are the same. This concept of sequence invariance applies to the case of Fig. 4b. Nonetheless, the sequences are different in both of these cases, hence, instigating the need to distinguish them.

4.1. Period-1 fixed points

Fixed points refer to the value of the state vector under steady state operation. Their calculation is important since the information that will be provided on the value of the duty cycle and state vector will be utilized in the formation of the Jacobian of the first return maps Gelig and Churilov (1998) and Zhusubaliyev, Soukhoterina and Mosekilde (2001). This subsection considers the period-1 orbit, in which case if one takes into account the symmetry of the system it can be deduced that the duty cycles provided by the controllers have the same values under steady state operation, i.e. $d_1 = d_2 = d$. The sequence of changing topologies then depends only on the value of the duty cycle d and is summarized in Table 2. To calculate the fixed points as a function of d , i.e. $x_0(d)$, the state transitions are utilized as shown in (5) and (6)¹

¹ The subscripts of the state transition matrices and convolution integrals are in direct correspondence with the matrices in (4).

for the case of $d \geq 0.5$.

$$x((d - 0.5)T) = \Phi_1(0, (d - 0.5)T)x(0) + \mathbf{I}_1(0, (d - 0.5)T) \quad (5)$$

$$x\left(\frac{T}{2}\right) = \Phi_3\left((d - 0.5)T, \frac{T}{2}\right)x((d - 0.5)T) + \mathbf{I}_3\left((d - 0.5)T, \frac{T}{2}\right) \quad (6)$$

Where the state transition matrices and convolution integrals are given below

$$\Phi_1(0, (d - 0.5)T) = e^{\mathbf{A}_1 t} \Big|_{t=(d-0.5)T}$$

$$\mathbf{I}_1(0, (d - 0.5)T) = \int_0^t e^{\mathbf{A}_1(t-\tau)} \mathbf{B}V_{in} d\tau \Big|_{t=(d-0.5)T}$$

$$\Phi_3\left((d - 0.5)T, \frac{T}{2}\right) = e^{\mathbf{A}_3 t} \Big|_{t=(1-d)T}$$

$$\mathbf{I}_3\left((d - 0.5)T, \frac{T}{2}\right) = \int_0^t e^{\mathbf{A}_3(t-\tau)} \mathbf{B}V_{in} d\tau \Big|_{t=(1-d)T}$$

At this point, although in the middle of the cycle, $x_0(d)$ can be defined by making the observation, which stems from the fact that there is symmetry both between the phases as well as in the current distribution among them, that there is relationship between $x(0)$ and $x\left(\frac{T}{2}\right)$ that is defined in (7).

$$x\left(\frac{T}{2}\right) = \begin{bmatrix} 1 & 0 & 0 \\ 0 & 0 & 1 \\ 0 & 1 & 0 \end{bmatrix} x(0) \quad (7)$$

Making use of (7), (5), (6) and applying periodicity, which means solving for $x(0)$, the steady state vector as a function of d can be defined in (8).²

$$x_{0,1}(d) = \left(\begin{bmatrix} 1 & 0 & 0 \\ 0 & 0 & 1 \\ 0 & 1 & 0 \end{bmatrix} - \Phi_3 \Phi_1 \right)^{-1} (\Phi_3 \mathbf{I}_1 + \mathbf{I}_3) \quad (8)$$

For the case of $d < 0.5$ a similar procedure is to be followed which will produce (9).

$$x_{0,2}(d) = \left(\begin{bmatrix} 1 & 0 & 0 \\ 0 & 0 & 1 \\ 0 & 1 & 0 \end{bmatrix} - \Phi_4 \Phi_2 \right)^{-1} (\Phi_4 \mathbf{I}_2 + \mathbf{I}_4) \quad (9)$$

Eqs. (8) and (9) are then utilized along with control law to provide Eq. (10), in which $i = 1, 2$, for the two different cases of the duty cycle. These equations are solved numerically to provide the duty cycles.

$$f(d) = -d - [k_1 \quad k_2] \left(\mathbf{C}_i x_{0,i}(d) - \begin{bmatrix} V_{ref} \\ I_{ref} \end{bmatrix} \right) + d_{ss} \quad (10)$$

$$\mathbf{C}_1 = \begin{bmatrix} 1 & 0 & 0 \\ 0 & 1 & 0 \end{bmatrix}, \quad \mathbf{C}_2 = \begin{bmatrix} 1 & 0 & 0 \\ 0 & 0 & 1 \end{bmatrix}$$

Matrices $\mathbf{C}_1, \mathbf{C}_2 \in \mathbb{R}^{2 \times 3}$ are utilized to specify which states among the state vector $x_{0,i}(d)$ are responsible for the determination of the switching condition.

4.2. Period-11 fixed points

The process of calculating the fixed points that correspond to the period-11 orbits is more challenging, however, by once again utilizing the symmetry of the system allows us to greatly reduce the amount calculations. Thus, the map from the beginning to the middle of the eleven period cycle's traversal is given in (11), where Φ_{p11}^{11} and \mathbf{I}_{p11}^{11} correspond to the expressions given in (12) and (13) respectively for $N = 11$. These expression are functions of the duty cycles d_j for

² The independent variables of the state transition matrices and convolution integrals are omitted due to space limitations.

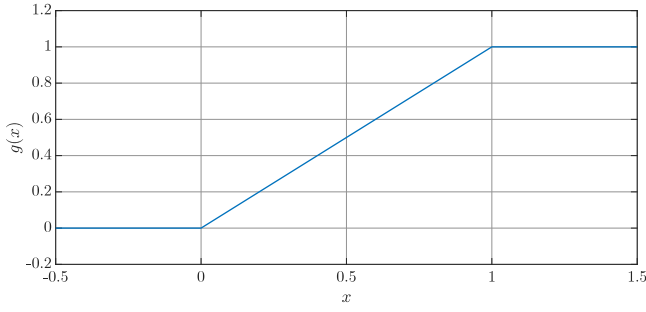


Fig. 5. Saturation function for $a = 5.10^3$.

$j = 1, 2, \dots, 11$ and describe the evolution of the system from time $t = 0$ to $t = NT/2$.

$$\mathbf{x}\left(5T + \frac{T}{2}\right) = \Phi_{P11}^{11} \mathbf{x}(0) + \mathbf{I}_{P11}^{11} \quad (11)$$

$$\Phi_{P11}^N\left(0, N\frac{T}{2}\right) = \prod_{j=N}^1 \Phi_{j \bmod 2+2}((1-d_j)T) \Phi_1((d_j-0.5)T) \quad (12)$$

$$\begin{aligned} \mathbf{I}_{P11}^N\left(0, N\frac{T}{2}\right) &= \sum_{i=1}^{N-1} \prod_{j=N}^{i+1} \Phi_{j \bmod 2+2}((1-d_j)T) \Phi_1((d_j-0.5)T) \times \\ &(\Phi_{i \bmod 2+2}((1-d_i)T) \mathbf{I}_1((d_i-0.5)T) + \mathbf{I}_{i \bmod 2+2}((1-d_i)T)) + \\ &\Phi_{N \bmod 2+2}((1-d_N)T) \mathbf{I}_1((d_N-0.5)T) + \mathbf{I}_{N \bmod 2+2}((1-d_N)T) \end{aligned} \quad (13)$$

The rest of the evolution up to $t = 11T$ is symmetric to (11) as far as the inductor currents are concerned with the voltage being identical. Thus the relationship between the state vector for the aforementioned time instances is

$$\mathbf{x}(5T + T/2) = \mathbf{M}_m \mathbf{x}(11T) \quad (14)$$

Substitution of (14) in (11) and enforcing periodicity, i.e. $\mathbf{x}(11T) = \mathbf{x}(0)$ in steady state operation, provides

$$\mathbf{M}_m \mathbf{x}(0) = \Phi_{P11}^{11} \mathbf{x}(0) + \mathbf{I}_{P11}^{11} \quad (15)$$

This is an over defined system of nonlinear equation with fourteen unknowns, namely three unknowns corresponding to the states at $t = 0$ represented by $\mathbf{x}(0)$ and the eleven duty cycles contained in Φ_{P11}^{11} and \mathbf{I}_{P11}^{11} . In order to provide the additional conditions to explicate the system the control laws are utilized in (16) which yields expressions that are directly related to the duty cycles. In Eq. (16a) $l = 1, 2, \dots, 10$ and $\mathbf{x}((l-1)T/2)$ can be found by making use of (13) and (12) for $N = l - 1$. It should be noted that $\Phi_{P11}^0 = \mathbf{I}_3$ and $\mathbf{I}_{P11}^0 = \mathbf{0}^T$.

$$\sigma_l = -d_{l+1} + g\left(-[k_1 \quad k_2] \left(\mathbf{C}_{(l+1) \bmod 2+1} \mathbf{x}\left((l-1)\frac{T}{2}\right) - \begin{bmatrix} V_{ref} \\ I_{ref} \end{bmatrix}\right) + d_{ss}\right) \quad (16a)$$

$$\sigma_{11} = -d_1 + g\left(-[k_1 \quad k_2] \left(\mathbf{C}_1 \mathbf{x}(5T) - \begin{bmatrix} V_{ref} \\ I_{ref} \end{bmatrix}\right) + d_{ss}\right) \quad (16b)$$

Moreover, the function $g(x)$ given in (17) is utilized in (16) in order to curtail the possible values of the duty cycles between 0 and 1 which will in turn facilitate numerical calculations. Fig. 5 illustrates this concept.

$$g(x) = x - \left(\frac{x}{1 + e^{ax}} + \frac{x-1}{1 + e^{-a(x-1)}}\right) \quad (17)$$

Eqs. (15) in conjunction with (16a) and (16b) constitute an explicit system of nonlinear algebraic equation, with the unknowns being the states $\mathbf{x}(0)$ at the beginning of the eleven period cycle and the eleven

duty cycles d_j for $j = 1, 2, \dots, 11$, which is solve by means of numerical methods.

4.3. Jacobian of the period-1 map

After the provision of the methods that are able to provide the fixed points of the system for both the period-1 and period-11 orbits in the previous Sections 4.1 and 4.2 respectively, their stability will be investigated by deriving the Jacobian matrices of the Poincaré maps for each case. In this subsection we will concern ourselves with the period-1 orbit. The analysis will be divided in two parts, namely one will be dealing with the duty cycle being smaller than 0.5, Section 4.3.1, and the other, Section 4.3.2, when it exceeds it. In the latter case, which represents the main contribution of this work, the map is extended to accommodate difference equations that describe the evolution of the control laws. The reason behind this is that the control laws depend upon past states, meaning that they are sampled and formed outside the time span of interest which is the period T of the cycle, and impede the perturbed representation of the first return map, i.e. the Monodromy matrix.

Furthermore, in Section 4.4, the proposed method is further validated by applying it to the period-11 orbit, since it occurs for all its duty cycles being above the threshold of 0.5, and allows to obtain information on its stability.

4.3.1. Case of $d < 0.5$

In the case where the duty cycle is below 0.5 the control law, which reflects the duty cycles, is formed twice in a period T . Namely once at time $t = 0$ corresponding to the first switch and at time $t = T/2$ for the second. The duty cycles in the aforementioned two cases are d_1 and d_2 respectively. This concept is depicted in Fig. 4a where at $t = 0$ duty cycle d_1 is formed which gives rise a change in the state of the first switch at time $d_1 T$. Moreover, at time $t = T/2$ the second duty cycle d_2 is formed which causes the second switch to change state at time $T/2 + d_2 T$.

Given the initial condition x_n the local mappings of the state vector from time $t = 0$ to $t = T/2$ and from $t = T/2$ to $t = T$ are given in (18) and (19) respectively.

$$\begin{aligned} \mathbf{P}_1(x_n, d_1) &= \Phi_4((0.5-d_1)T) \Phi_3(d_1 T) x_n + \\ &\Phi_4((0.5-d_1)T) \mathbf{I}_3(d_1 T) + \mathbf{I}_4((0.5-d_1)T) \end{aligned} \quad (18)$$

$$\begin{aligned} \mathbf{P}_2(x(T/2), d_2) &= \Phi_4((0.5-d_2)T) \Phi_2(d_2 T) x(T/2) + \\ &\Phi_4((0.5-d_2)T) \mathbf{I}_2(d_2 T) + \mathbf{I}_4((0.5-d_2)T) \end{aligned} \quad (19)$$

The composition of the above two maps $\mathbf{P}(x_n, d_1, d_2) = \mathbf{P}_2(x(T/2), d_2) \circ \mathbf{P}_1(x(0), d_1)$ can describe the transition of the state vector in the time span T of the orbital cycle (Aroudi, Debbat, & Martinez-Salamero, 2007). The result of the composition is shown in (20), (21) and (22).

$$\mathbf{P}(x_n, d_1, d_2) = \Phi(d_1, d_2) x_n + \Psi(d_1, d_2) \quad (20)$$

$$\Phi(d_1, d_2) = \Phi_4((0.5-d_2)T) \Phi_2(d_2 T) \Phi_4((0.5-d_1)T) \Phi_3(d_1 T) \quad (21)$$

$$\begin{aligned} \Psi(d_1, d_2) &= \Phi_4((0.5-d_2)T) \Phi_2(d_2 T) \Phi_4((0.5-d_1)T) \mathbf{I}_3(d_1 T) \\ &+ \Phi_4((0.5-d_2)T) \Phi_2(d_2 T) \mathbf{I}_4((0.5-d_1)T) + \\ &\Phi_4((0.5-d_2)T) \mathbf{I}_2(d_2 T) + \mathbf{I}_4((0.5-d_2)T) \end{aligned} \quad (22)$$

The stability of $\mathbf{P}(x_n, \mathbf{d})$, where $\mathbf{d} = [d_1 \ d_2]^T$, is decided upon by taking its Jacobian with respect to x_n , i.e. $\mathbf{DP}(x_n, \mathbf{d})$. This matrix describes the evolution of a perturbation from the beginning of the cycle to its end and it is given in (23).

$$\mathbf{DP}(x_n, \mathbf{d}) = \frac{\partial \mathbf{P}(x_n, \mathbf{d})}{\partial x_n} + \frac{\partial \mathbf{P}(x_n, \mathbf{d})}{\partial \mathbf{d}} \frac{\partial \mathbf{d}}{\partial x_n} \quad (23)$$

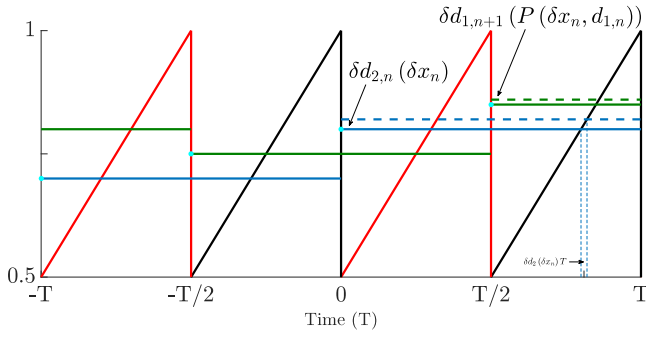


Fig. 6. Operation of the control signals in the case of $d \geq 0.5$. The black and red triangular traces represent the carrier signals for the first and second switch respectively. The blue and green traces correspond to the control laws of the first and second switch while their dashed versions are under the effect of a perturbation. The instances that they are formed, i.e. when the state vector is sampled, are represented with cyan dots. (For interpretation of the references to colour in this figure legend, the reader is referred to the web version of this article.)

As one can discern the expression for $\mathbf{DP}(x_n, \mathbf{d})$ also includes the derivative of \mathbf{d} with respect x_n . The reason is that \mathbf{d} is a function of x_n which directly relates to the control laws. Namely, the two control laws in this case are given in (24).

$$\mathbf{s}(x_n, \mathbf{d}) = \begin{bmatrix} -[k_1 \quad k_2] \left(\mathbf{C}_1 x_n - \begin{bmatrix} V_{ref} \\ I_{ref} \end{bmatrix} \right) + d_{ss} \\ -[k_1 \quad k_2] \left(\mathbf{C}_1 \mathbf{P}_1(x_n, d_1) - \begin{bmatrix} V_{ref} \\ I_{ref} \end{bmatrix} \right) + d_{ss} \end{bmatrix} \quad (24)$$

However, the aforementioned differentiation cannot be done explicitly because $\mathbf{s}(x_n, \mathbf{d})$ has a nonlinear dependence on \mathbf{d} . What come to our rescue is the implicit function and the switching manifolds. The switching manifolds are $\sigma(x_n, \mathbf{d}) = \mathbf{d} - \mathbf{s}(x_n, \mathbf{d}) = 0$ and the implicit function theorem allows us to recast (23) as shown in (25).

$$\mathbf{DP}(x_n, \mathbf{d}) = \frac{\partial \mathbf{P}(x_n, \mathbf{d})}{\partial x_n} - \frac{\partial \mathbf{P}(x_n, \mathbf{d})}{\partial \mathbf{d}} \left(\frac{\partial \sigma(x_n, \mathbf{d})}{\partial \mathbf{d}} \right)^{-1} \frac{\partial \sigma(x_n, \mathbf{d})}{\partial x_n} \quad (25)$$

The above Jacobian matrix is evaluated at the fixed points derived in the previous section and its eigenvalues provide information on the orbital stability.

4.3.2. Case of $d \geq 0.5$

In the case where the duty cycle d has a larger value than 0.5 one of the control laws is formed outside the period of the cycle under consideration, i.e. T . For example, referring to Fig. 4b in the span of $t \in [0, T]$, it can be seen that the switching condition for the second switch is formed at $t = -T/2$, suggesting an independence of the control law from the state vector $x(t)$ for $t \in [0, T]$. This is the exact point where the conventional approach of 4.3.1 fails since the switching manifolds are contingent to x_n , which should lay inside the span of the cycle. The reader is referred to Fig. 6 for a concise explanation. As it can be seen, when a perturbation comes at $t = 0$ it only affects the control signal that corresponds to the first controller. This is connoted in the figure by $\delta d_{2,n}(\delta x_n)$ where δx_n is the perturbation. The effects of the perturbation on the second controller, depicted as $\delta d_{1,n+1}(\mathbf{P}(\delta x_n, d_{1,n}))$ in the figure, will become apparent at $t = T/2$ which will, however, have no impact on this cycle but the next.

The conventional approach of the Poincaré map, as was implemented in 4.3.1, makes use of switching manifolds that depend on the state vector x_n and not on its previous instances. This problematic situation is ameliorated by incorporating the control laws into the discrete map as difference equations that are able to precisely describe their evolution in time. This formulation alleviates their dependence on the state vector outside the cycle, thus, enabling us to derive the

appropriate Monodromy Matrix and deciding upon the stability of the orbit. The extended first return map that accommodates the difference equation concerning the duty cycles is given in (26)³ which constitutes a nonlinear system of difference equations.

$$\begin{aligned} x_{n+1} &= \Phi_{P_1}^2 x_n + \mathbf{I}_{P_1}^2 \\ \mathbf{d}_{1,n+1} &= -[k_1 \quad k_2] \left(\mathbf{C}_2 (\Phi_{P_1}^1 x_n + \mathbf{I}_{P_1}^1) - \begin{bmatrix} V_{ref} \\ I_{ref} \end{bmatrix} \right) + d_{ss} \\ \mathbf{d}_{2,n+1} &= -[k_1 \quad k_2] \left(\mathbf{C}_1 (\Phi_{P_1}^1 x_n + \mathbf{I}_{P_1}^1) - \begin{bmatrix} V_{ref} \\ I_{ref} \end{bmatrix} \right) + d_{ss} \end{aligned} \quad (26)$$

System (26) contains all the information that describe the effects of the states on the control laws and, concomitantly, on the duty cycles. In comparison to the conventional procedure undertaken in Section 4.3.1 this effect had to be unveiled by considering expression that involved switching manifolds and their derivatives with respect to both the states and duty cycles, cf. Eq. (25). Involved calculations like those can be dispensed with in this case since a linearization of (26) around the point of interest will provide information on the stability of the limit cycle. The linearized map, $\mathbf{DP}(x_n, \mathbf{d}_n)$, is given below and its entries are denoted in (27).

$$\mathbf{DP}(x_n, \mathbf{d}_n) = \begin{bmatrix} \frac{\partial x_{n+1}}{\partial x_n} & \frac{\partial x_{n+1}}{\partial \mathbf{d}_{1,n}} & \frac{\partial x_{n+1}}{\partial \mathbf{d}_{2,n}} \\ \frac{\partial \mathbf{d}_{1,n+1}}{\partial x_n} & \frac{\partial \mathbf{d}_{1,n+1}}{\partial \mathbf{d}_{1,n}} & \frac{\partial \mathbf{d}_{1,n+1}}{\partial \mathbf{d}_{2,n}} \\ \frac{\partial \mathbf{d}_{2,n+1}}{\partial x_n} & \frac{\partial \mathbf{d}_{2,n+1}}{\partial \mathbf{d}_{1,n}} & \frac{\partial \mathbf{d}_{2,n+1}}{\partial \mathbf{d}_{2,n}} \end{bmatrix}$$

$$\frac{\partial x_{n+1}}{\partial x_n} = \Phi_2((1-d)T) \Phi_1((d-0.5)T) \Phi_3((1-d)T) \Phi_1((d-0.5)T)$$

$$\frac{\partial x_{n+1}}{\partial \mathbf{d}_{1,n}} = \Phi_2((1-d)T) \Phi_1((d-0.5)T) \Phi_3((1-d)T) (\mathbf{A}_1 - \mathbf{A}_3) \mathbf{x} \times ((d-0.5)T)$$

$$\frac{\partial x_{n+1}}{\partial \mathbf{d}_{2,n}} = \Phi_2((1-d)T) (\mathbf{A}_1 - \mathbf{A}_2) \mathbf{x} (dT)$$

$$\frac{\partial \mathbf{d}_{1,n+1}}{\partial x_n} = -\mathbf{k} \mathbf{C}_2 \Phi_3((1-d)T) \Phi_1((d-0.5)T)$$

$$\frac{\partial \mathbf{d}_{1,n+1}}{\partial \mathbf{d}_{1,n}} = -\mathbf{k} \mathbf{C}_2 \Phi_3((1-d)T) (\mathbf{A}_1 - \mathbf{A}_3) \mathbf{x} ((d-0.5)T)$$

$$\frac{\partial \mathbf{d}_{1,n+1}}{\partial \mathbf{d}_{2,n}} = 0$$

$$\frac{\partial \mathbf{d}_{2,n+1}}{\partial x_n} = -\mathbf{k} \mathbf{C}_1 \frac{\partial x_{n+1}}{\partial x_n}$$

$$\frac{\partial \mathbf{d}_{2,n+1}}{\partial \mathbf{d}_{1,n}} = -\mathbf{k} \mathbf{C}_1 \frac{\partial x_{n+1}}{\partial \mathbf{d}_{1,n}}$$

$$\frac{\partial \mathbf{d}_{2,n+1}}{\partial \mathbf{d}_{2,n}} = -\mathbf{k} \mathbf{C}_1 \frac{\partial x_{n+1}}{\partial \mathbf{d}_{2,n}} \quad (27)$$

The above expression for the linearized first return map is calculated at the point of interest which can be derived by following the procedure in Section 4.1. The results of this operation are presented in Table 3 in which the first two rows foresee the Neimark–Sacker bifurcation. The bifurcation criterion is associated with the scalar value k which when it attains the value 0.9333 two complex eigenvalues escape the unit cycle. This is shown in Fig. 2. In addition, the last two rows identify the point where the system undergoes a saddle–node bifurcation for $k = 0.7765$. The latter is a common trait of the boost converter as shown in Giaouris et al. (2013).

³ The subscript \mathbf{P}_1 connotes the fact that only a period-1 orbit is considered and is in direct correspondence with (12) and (13) for $N = 2$.

Table 3
Monodromy matrix eigenvalues.

k	d	$x(0)$	Eigenvalues	$\ \cdot \ _2$
0.933	0.9922	$\begin{bmatrix} 53.9704 \\ 8.4628 \\ 8.5666 \end{bmatrix}$	$\begin{bmatrix} 0 \\ 0.9901 \\ 0.7266 \\ -0.6578 \pm i0.7520 \end{bmatrix}$	$\begin{bmatrix} 0 \\ 0.9901 \\ 0.7266 \\ 0.9992 \end{bmatrix}$
0.9333	0.9922	$\begin{bmatrix} 53.9717 \\ 8.4713 \\ 8.5750 \end{bmatrix}$	$\begin{bmatrix} 0 \\ 0.9901 \\ 0.7266 \\ -0.6591 \pm i0.7526 \end{bmatrix}$	$\begin{bmatrix} 0 \\ 0.9901 \\ 0.7266 \\ 1.0005 \end{bmatrix}$
0.7765	0.8450	$\begin{bmatrix} 30.9816 \\ 2.3707 \\ 2.4896 \end{bmatrix}$	$\begin{bmatrix} 0 \\ 1.0012 \\ 0.7857 \\ 0.1291 \pm i0.1965 \end{bmatrix}$	$\begin{bmatrix} 0 \\ 1.0012 \\ 0.7857 \\ 0.2351 \end{bmatrix}$
0.7765	0.8553	$\begin{bmatrix} 32.9608 \\ 2.7146 \\ 2.8327 \end{bmatrix}$	$\begin{bmatrix} 0 \\ 0.9989 \\ 0.7755 \\ 0.0916 \pm i0.2529 \end{bmatrix}$	$\begin{bmatrix} 0 \\ 0.9989 \\ 0.7755 \\ 0.2690 \end{bmatrix}$

4.4. Jacobian of the p -11 map

The process of calculating the Jacobian of the period-11 map is more laborious in comparison to the preceding subsections, however, it will further validate the proposed method in 4.3.2 and further alleviate cogency by undertaking it.

As it has been suggested in Section 4.2 by Eq. (15) the symmetry of the system can work in our favour when it comes to calculating the steady-state state vector by diminishing the extend that (12) would have taken otherwise. However, in this case where we need to derive the Jacobian of the period-11 map the transition of the state vector in the whole span of the eleven periods has to be taken under consideration. Fortunately, a systematic way can be deduced that will provide the desired results on the stability of the sizeable orbit. Having said that, the map that describes the evolution of the state vector is shown in (28). In this case, vector \mathbf{d} is comprised of 22 entries, i.e. $\mathbf{d} = [d_1, d_2, \dots, d_{22}]^T$, however due to symmetry $d_i = d_{i+11}$ for $i = 1, 2, \dots, 11$. Furthermore, the most salient aspects is the denotation of the switching manifolds and the augmentation of the map with the difference equation that describes the evolution of the duty cycle, in this case d_1 , that has a dependence on samples of the state vector before the beginning of the cycle. The latter has been illustrated in Section 4.3.2 for the case of the period-1 map and needs to also be employed in this case since the period-11 orbit takes place for values of the duty cycles being above 0.5. Thus, the system (28) will be augmented with (29)⁴ and will be denoted as $\mathbf{P}_a(\mathbf{d}, \mathbf{x}_n)$. The entries of the vector that is comprised by the switching manifolds, i.e. $\sigma(\mathbf{d}, \mathbf{x}_n)$, can be constructed by (16a) for $l = 1, 2, \dots, 21$.

$$\mathbf{P}(\mathbf{d}, \mathbf{x}_n) = \Phi_{P11}^{22} \mathbf{x}_n + \mathbf{I}_{P11}^{22} \quad (28)$$

$$d_{1,n+1} = g \left(- \begin{bmatrix} k_1 & k_2 \end{bmatrix} \left(\mathbf{C}_1 \left(\Phi_{P11}^{21} \mathbf{x}_n + \mathbf{I}_{P11}^{21} \right) - \begin{bmatrix} V_{ref} \\ I_{ref} \end{bmatrix} \right) + d_{ss} \right) \quad (29)$$

The Jacobian $\mathbf{DP}_a(\mathbf{d}, \mathbf{x}_n)$ will be constructed in accordance with (25). However, due to the nature of the augmented map the new state vector is $\tilde{\mathbf{x}}_n = [\mathbf{x}_n, d_1]^T$. Hence, the Jacobian of $\mathbf{P}_a(\mathbf{d}, \mathbf{x}_n)$ with respect to $\tilde{\mathbf{x}}_n$ is given in (31) with its relevant entries being expressed in (35) to (38) where $\Xi^{N,M}$ is defined in (30).

$$\Xi^{N,M} = \prod_{j=N}^M \Phi_{j \bmod 2+2} \left((1-d_j)T \right) \Phi_1 \left((d_j-0.5)T \right) \quad (30)$$

⁴ At this point it should be noted that the use of (17) is essential since some of the duty cycles are saturated. Further elaboration on this will be given subsequently.

$$\frac{\partial \mathbf{DP}_a(\mathbf{d}, \mathbf{x}_n)}{\partial \tilde{\mathbf{x}}_n} = \begin{bmatrix} \frac{\partial \mathbf{P}(\mathbf{d}, \mathbf{x}_n)}{\partial \mathbf{x}_n} & \frac{\partial \mathbf{P}(\mathbf{d}, \mathbf{x}_n)}{\partial d_1} \\ \frac{\partial d_{1,n+1}}{\partial \mathbf{x}_n} & \frac{\partial d_{1,n+1}}{\partial d_1} \end{bmatrix} \quad (31)$$

The next term to be calculated is the Jacobian of the augmented map with respect to the duty cycles d_k , $k = 2, 3, \dots, 22$ which belongs in $\mathbb{R}^{4 \times 21}$. Its column entries are given in (32) and they are calculated with the assistance of (39) and (40).⁵

$$\frac{\partial \mathbf{DP}_a(\mathbf{d}, \mathbf{x}_n)}{\partial d_k} = \begin{bmatrix} \frac{\partial \mathbf{P}(\mathbf{d}, \mathbf{x}_n)}{\partial d_k} \\ \frac{\partial d_{1,n+1}}{\partial d_k} \end{bmatrix} \quad (32)$$

What remains to conclude the assembly of $\mathbf{P}_a(\mathbf{d}, \mathbf{x}_n)$ is the derivation of the Jacobians of the switching manifolds $\sigma(\mathbf{d}, \mathbf{x}_n)$ with respect to $\tilde{\mathbf{x}}_n$ and d_k , $k = 2, 3, \dots, 22$. To this end, and in order to facilitate a succinct formulation, what will be dealt with first is the switching functions of the switching manifolds, i.e. $s(\mathbf{x}_n, \mathbf{d})$ which are in congruence with the control laws. If $\tilde{\mathbf{d}}$ is let to be the aggregate of the duty cycles that correspond to the switching functions, i.e. $\tilde{\mathbf{d}} = [d_2, d_3, \dots, d_{22}]^T$, then the pertinent Jacobians are $\partial s(\mathbf{x}_n, \mathbf{d}) / \partial \tilde{\mathbf{d}} \in \mathbb{R}^{21 \times 21}$ and $\partial s(\mathbf{x}_n, \mathbf{d}) / \partial \tilde{\mathbf{x}}_n \in \mathbb{R}^{21 \times 4}$. Each scalar entry of $\partial s(\mathbf{x}_n, \mathbf{d}) / \partial \tilde{\mathbf{d}}$ is given in (41) for $1 \leq l \leq 21$, $2 \leq k \leq 22$. Moreover, $\partial s(\mathbf{x}_n, \mathbf{d}) / \partial \tilde{\mathbf{x}}_n$ can be decomposed as shown in (33).

$$\frac{\partial s(\mathbf{x}_n, \mathbf{d})}{\partial \tilde{\mathbf{x}}_n} = \begin{bmatrix} \frac{\partial s(\mathbf{x}_n, \mathbf{d})}{\partial \mathbf{x}_n} & \frac{\partial s(\mathbf{x}_n, \mathbf{d})}{\partial d_1} \end{bmatrix} \quad (33)$$

The first and second term on the right of (33) can be constructed by utilizing (41) and (42) respectively. In both cases $1 \leq l \leq 21$ and in the second $k = 1$.

At this point all the parts that comprise $\mathbf{DP}_a(\mathbf{d}, \mathbf{x}_n)$ have been obtained which allows it to be expressed as in (34).

$$\mathbf{DP}_a(\mathbf{d}, \mathbf{x}_n) = \frac{\partial \mathbf{P}_a(\mathbf{d}, \mathbf{x}_n)}{\partial \tilde{\mathbf{x}}_n} - \frac{\partial \mathbf{P}_a(\mathbf{d}, \mathbf{x}_n)}{\partial \tilde{\mathbf{d}}} \left(-\mathbf{I}_{21} + \frac{\partial s(\mathbf{x}_n, \mathbf{d})}{\partial \tilde{\mathbf{x}}_n} \right)^{-1} \frac{\partial s(\mathbf{x}_n, \mathbf{d})}{\partial \tilde{\mathbf{x}}_n} \quad (34)$$

In reference to Fig. 3a, Table 4 presents the eigenvalues of (34) for the unstable and stable periodic orbits. At this point for k approximately equal to 0.938 a saddle-node bifurcation takes place since two eigenvalues have broken away from the point $1 + j0$ on the unit cycle. One eigenvalue traverses inwards and the other outwards of the unit cycle along the real axis.

$$\frac{\partial \mathbf{P}(\mathbf{d}, \mathbf{x}_n)}{\partial \mathbf{x}_n} = \Phi_{P11}^{22} \quad (35)$$

$$\frac{\partial \mathbf{P}(\mathbf{d}, \mathbf{x}_n)}{\partial d_1} = \Xi^{22,2} \Phi_3 \left((1-d_1)T \right) \left(\mathbf{A}_4 - \mathbf{A}_3 \right) \mathbf{x} \left((d_1-0.5)T \right) \quad (36)$$

$$\frac{\partial d_{1,n+1}}{\partial \mathbf{x}_n} = - \begin{bmatrix} k_1 & k_2 \end{bmatrix} \mathbf{C}_1 \Xi^{21,1} g'(d_1) \quad (37)$$

$$\frac{\partial d_{1,n+1}}{\partial d_1} = - \begin{bmatrix} k_1 & k_2 \end{bmatrix} \mathbf{C}_1 \Xi^{21,2} \Phi_3 \left((1-d_1)T \right) \left(\mathbf{A}_4 - \mathbf{A}_3 \right) \mathbf{x} \times \left((d_1-0.5)T \right) g'(d_1) \quad (38)$$

$$\frac{\partial \mathbf{P}(\mathbf{d}, \mathbf{x}_n)}{\partial d_k} = \begin{cases} \Xi^{22,k+1} \Phi_{k \bmod 2+2} \left((1-d_k)T \right) \left(\mathbf{A}_4 - \mathbf{A}_{k \bmod 2+2} \right) \mathbf{x} \\ \times \left((d_k-0.5)T + (k-1)T/2 \right), 2 \leq k \leq 21 \\ \Phi_{k \bmod 2+2} \left((1-d_k)T \right) \left(\mathbf{A}_4 - \mathbf{A}_{k \bmod 2+2} \right) \mathbf{x} \left((d_k-0.5)T \right. \\ \left. + (k-1)T/2 \right), k = 22 \end{cases} \quad (39)$$

⁵ $g'(x)$ connotes the derivative of $g(x)$ with respect to x .

Table 4
Monodromy matrix eigenvalues for the period-11 orbit and $k = 0.938$.

k	d	$x(0)$	Eigenvalues	$\ \cdot \ _2$
0.938	0.9448	$\begin{bmatrix} 55.6670 \\ 8.4203 \\ 8.5675 \end{bmatrix}$	$\begin{bmatrix} 1.2169 \\ 0.8906 \\ 0 \\ 0.0984 \end{bmatrix}$	$\begin{bmatrix} 1.2169 \\ 0.8906 \\ 0 \\ 0.0984 \end{bmatrix}$
	1.0000			
	0.9688			
	0.8842			
	0.8428			
	0.8963			
	0.9813			
	0.9982			
	0.9250			
	0.8489			
	0.8584			
0.938	0.9408	$\begin{bmatrix} 55.6445 \\ 8.4174 \\ 8.5710 \end{bmatrix}$	$\begin{bmatrix} 0.8893 \\ 0.3862 \\ 0 \\ 0.0676 \end{bmatrix}$	$\begin{bmatrix} 0.8893 \\ 0.3862 \\ 0 \\ 0.0676 \end{bmatrix}$
	1.0000			
	0.9725			
	0.8871			
	0.8416			
	0.8923			
	0.9792			
	1.0000			
	0.9291			
	0.8506			
	0.8556			

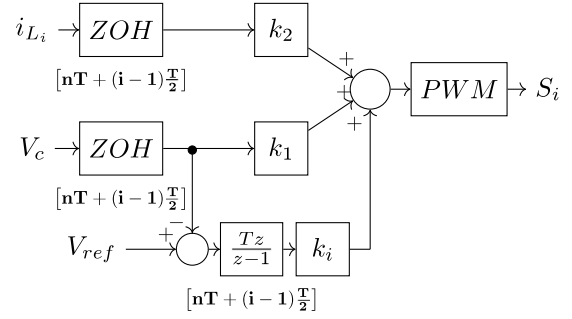
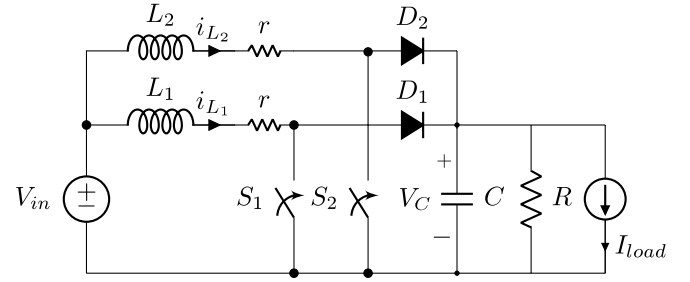


Fig. 7. Two-legged interleaved DC-DC boost converter with dynamic state feedback controller.

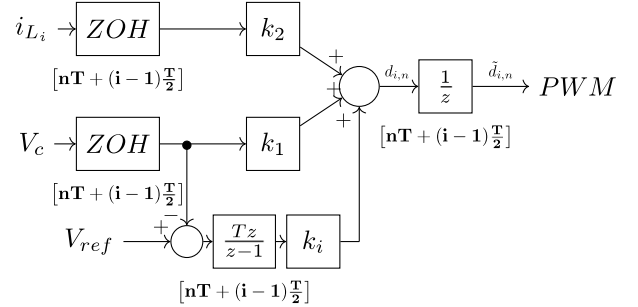


Fig. 8. Dynamic state-feedback controller with on sample delay.

the current source, I_{load} , will serve as the bifurcation parameter. The control gain vector $\mathbf{k} = [0.1496 \ 2 \ -808]$, which was acquired based on the analysis conducted in Gkizas et al. (2018), aims to provide the system with a large damping factor and natural frequency, namely $\zeta = 0.7$ and $\omega_n = 7000$ r/s respectively as far as the dominant poles are concerned, at the operating point of 10V whilst the current sink is sourcing 1 A.

The analysis commences by forming a first return map that describes the evolution of the states in a single cycle. In the case where both the duty cycles of the converter are above the 0.5 threshold this is achieved with the map in (44). As it can be seen two additional states are introduced in the system to describe the operation of the integrators, which are portrayed in the control system at the bottom part of Fig. 7. Moreover, in order to incorporate the current sink in the first return map the input matrix \mathbf{B} , given in (4), is modified as shown in (43) and the input to the system is $[V_{in}, I_{load}]$.

$$\mathbf{B} = \begin{bmatrix} -1/C & 0 & 0 \\ 0 & 1/L & 1/L \end{bmatrix}^T \quad (43)$$

$$\frac{\partial d_{1,n+1}}{\partial d_k} = \begin{cases} -[k_1 \ k_2] \mathbf{C}_1 \Xi^{21,k+1} \Phi_{k \bmod 2+2} ((1-d_k)T) (\mathbf{A}_4 - \mathbf{A}_{k \bmod 2+2}) \mathbf{x} \\ \quad \times ((d_k - 0.5)T + (k-1)T/2) g'(d_1), \ 2 \leq k \leq 20 \\ -[k_1 \ k_2] \mathbf{C}_1 \Phi_{k \bmod 2+2} ((1-d_k)T) (\mathbf{A}_4 - \mathbf{A}_{k \bmod 2+2}) \mathbf{x} \\ \quad \times ((d_k - 0.5)T + (k-1)T/2) g'(d_1), \ k = 21 \\ 0, \ k = 22 \end{cases} \quad (40)$$

$$\frac{\partial s_l(\mathbf{d}, \mathbf{x}_n)}{\partial d_k} = \begin{cases} -[k_1 \ k_2] \mathbf{C}_{(l+1) \bmod 2+1} \Xi^{l-1,k+1} \Phi_{k \bmod 2+2} ((1-d_k)T) \\ \quad \times (\mathbf{A}_4 - \mathbf{A}_{k \bmod 2+2}) \mathbf{x} ((d_k - 0.5)T + (k-1)T/2) g'(d_{l+1}), \ k+1 < l \\ -[k_1 \ k_2] \mathbf{C}_{(l+1) \bmod 2+1} \Phi_{k \bmod 2+2} ((1-d_k)T) \\ \quad \times (\mathbf{A}_4 - \mathbf{A}_{k \bmod 2+2}) \mathbf{x} ((d_k - 0.5)T + (k-1)T/2) g'(d_{l+1}), \ k+1 = l \\ 0, \ k+1 > l \end{cases} \quad (41)$$

$$\frac{\partial s_l(\mathbf{d}, \mathbf{x}_n)}{\partial \mathbf{x}_n} = \begin{cases} -[k_1 \ k_2] \mathbf{C}_{(l+1) \bmod 2+1} \Xi^{l-1,1} g'(d_{l+1}), \ l > 1 \\ -[k_1 \ k_2] \mathbf{C}_{(l+1) \bmod 2+1} g'(d_{l+1}), \ l = 1 \end{cases} \quad (42)$$

5. Dynamic state feedback

Dynamic state feedback is ubiquitous technique employed in compensating power conversion systems as it can be deduced from a plethora of studies since it contributes several advantages. Amongst them the most noteworthy are the ability to diminish steady state error and ameliorate disturbances. In addition, when it comes to our case of the interleaved boost converter the multiple equilibria that would be present in the case of static control laws do not come into existence (Gkizas et al., 2016, 2018). This can be accounted to the operation of the integrator which curtails the system to only one equilibrium point. However, limit cycle instabilities are still present. This section will be concerned with the limit cycle stability analysis of the converter under dynamic state feedback and will extrapolate the ideas and results of Section 4.3.

The converter, along with the control system that comprises the dynamic state feedback control law, is depicted in Fig. 7 in which

Table 5
Monodromy matrix eigenvalues under dynamic state feedback.

I_{load}	d	$x(0)$	Eigenvalues	$\ \cdot \ _2$
0.0	0.5266	$\begin{bmatrix} 10 \\ 0.2119 \\ 0.3362 \end{bmatrix}$	$-0.1115 \pm i0.2046$	$\begin{bmatrix} 0.2330 \\ 0.0000 \\ 0.4679 \\ 0.7816 \\ 0.9888 \end{bmatrix}$
			0.0000 0.4679 $0.7650 \pm i0.1603$ 0.9888	
0.5	0.5308	$\begin{bmatrix} 10 \\ 0.7467 \\ 0.8697 \end{bmatrix}$	$-0.1013 \pm i0.3854$	$\begin{bmatrix} 0.3985 \\ 0 \\ 0.8380 \\ 0.8740 \\ 0.9887 \end{bmatrix}$
			0.0000 0.8380 $0.7563 \pm i0.4382$ 0.9887	
0.8443	0.5336	$\begin{bmatrix} 10 \\ 1.1204 \\ 1.2424 \end{bmatrix}$	$-0.0799 \pm i0.4824$	$\begin{bmatrix} 0.4890 \\ 0 \\ 0.8643 \\ 0.9999 \\ 0.9887 \end{bmatrix}$
			0 0.8643 $0.8532 \pm i0.5214$ 0.9887	
0.845	0.5336	$\begin{bmatrix} 10 \\ 1.1211 \\ 1.2432 \end{bmatrix}$	$-0.0798 \pm i0.4826$	$\begin{bmatrix} 0.4892 \\ 0 \\ 0.8644 \\ 1.0002 \\ 0.9887 \end{bmatrix}$
			0 0.8644 $0.8534 \pm i0.5215$ 0.9887	

Table 6
Monodromy matrix eigenvalues under dynamic state feedback with one sample delay.

I_{load}	d	$x(0)$	Eigenvalues	$\ \cdot \ _2$
0	0.5266	$\begin{bmatrix} 10 \\ 0.2119 \\ 0.3362 \end{bmatrix}$	0.0200	$\begin{bmatrix} 0.0200 \\ 1.0233 \\ 1.0683 \\ 0.8055 \\ 0.9888 \end{bmatrix}$
			$0.6111 \pm i0.8208$ $0.5293 \pm i0.9280$ $0.7930 \pm i0.1413$ 0.9888	
0.5	0.5308	$\begin{bmatrix} 10 \\ 0.7467 \\ 0.8697 \end{bmatrix}$	$0.1266 \pm i0.2925$	$\begin{bmatrix} 0.3187 \\ 1.0825 \\ 1.0140 \\ 0.9887 \\ 0.8307 \end{bmatrix}$
			$0.5779 \pm i0.9153$ $0.8241 \pm i0.5909$ 0.9887 0.8307	

$$\begin{aligned}
\mathbf{x}_{n+1} &= \Phi_{p1}^2 \mathbf{x}_n + \mathbf{I}_{p1}^2 \\
\mathbf{d}_{1,n+1} &= - [k_1 \quad k_2] C (\Phi_{p1}^1 \mathbf{x}_n + \mathbf{I}_{p1}^1) \\
&\quad - k_i T (\mathbf{x}_{5,n} - [1 \quad 0 \quad 0] (\Phi_{p1}^1 \mathbf{x}_n + \mathbf{I}_{p1}^1) + V_{ref}) \\
\mathbf{d}_{2,n+1} &= - [k_1 \quad k_2] C (\Phi_{p1}^2 \mathbf{x}_n + \mathbf{I}_{p1}^2) \\
&\quad - k_i T (\mathbf{x}_{4,n} - [1 \quad 0 \quad 0] (\Phi_{p1}^2 \mathbf{x}_n + \mathbf{I}_{p1}^2) + V_{ref}) \\
\mathbf{x}_{4,n+1} &= \mathbf{x}_{4,n} - [1 \quad 0 \quad 0] (\Phi_{p1}^2 \mathbf{x}_n + \mathbf{I}_{p1}^2) + V_{ref} \\
\mathbf{x}_{5,n+1} &= \mathbf{x}_{5,n} - [1 \quad 0 \quad 0] (\Phi_{p1}^1 \mathbf{x}_n + \mathbf{I}_{p1}^1) + V_{ref}
\end{aligned} \tag{44}$$

In order to investigate the stability of the orbit a similar procedure⁶ as in Section 4.3.2 takes place where the system (44) is linearized around the point of interest. The linearization in this case takes place with respect to the seven states described by (44). The process results in the acquisition of the Monodromy Matrix which can be utilized to precisely decide upon the stability of the limit cycle.

To this end, Table 5 summarizes some salient points of operation with respect to the Monodromy Matrix. As it can be seen while the bifurcation parameter, i.e. I_{load} , assumes larger values a pair of complex conjugate eigenvalues exit the unit circle for $I_{load} = 0.845$ giving rise to a Neimark–Sacker bifurcation. At this point, it is important to notice that although the system was designed to be stable around the point of interest, as described in the second paragraph of this section, the limit cycle stability is not guaranteed thus rendering the preceding analysis a necessity.

⁶ The result of the linearization procedure is omitted due to the extend of terms involved in the process.

The case mentioned above was concerned with $d_1, d_2 \geq 0.5$ since the desired reference point is 10 V. On the other hand, when $d_1, d_2 < 0.5$, the inference of the map is straightforward if one refers to Section 4.3.1. The first return map can be constructed by utilizing Eq. (20) along with (45)⁷ which describes the dynamics of the integrators. With the addition of the control laws in (46) the Jacobian can be readily derived.

$$\begin{aligned}
x_{4,n+1} &= x_{4,n} - [1 \quad 0 \quad 0] \mathbf{P}(\mathbf{x}_n, d_1, d_2) + V_{ref} \\
x_{5,n+1} &= x_{5,n} - [1 \quad 0 \quad 0] \mathbf{P}_1(\mathbf{x}_n, d_1) + V_{ref}
\end{aligned} \tag{45}$$

$$\mathbf{s}(\mathbf{x}_n, \mathbf{d}) = \begin{bmatrix} - [k_1 \quad k_2] C_1 \mathbf{x}_n - k_i T x_{4,n} \\ - [k_1 \quad k_2] C_2 \mathbf{P}_1(\mathbf{x}_n, d_1) - k_i T x_{5,n} \end{bmatrix} \tag{46}$$

Until this point it has been rigorously and cogently proven that there is plethora of instabilities in the system under consideration. Both static and dynamic state feedback control laws, although designed to provide the system with stability under the framework of the average model, can give rise to unpalatable phenomena that deteriorate the operation of the converter. What further remains is to investigate the implications that might stem from experimentally implementing the control laws. The purpose of investigating an experimental situation is to decide upon whether the limit cycle instabilities intensify or diminish. The next section will be dedicated to this endeavour.

6. Implementation considerations

The bifurcation analysis thus far, namely in Sections 4.3.2 and 5, provided a method that is able to overcome the problems instigated by interleaving in conjunction with digital control concerning the description of the first return map. That was achieved by augmenting the first return map with the necessary difference equations that describe the evolution of salient quantities such as the duty cycles and discrete integrators. Having said that, the formulation and underlying ideas of the aforementioned first return maps can provide useful insight on how to incorporate some additional characteristics of the control system that stem from the physical implementation of the control laws. The most important aspect is the one sample delay that comes from the implementation of the digital control. Specifically, in the vast majority of experimental implementations under the digital control framework the states are sampled and the duty cycle is formed by making use of the control law expression in a computational unit. However, the duty cycle calculated is enforced in the next sampling period hence giving rise to one period delay. Fig. 8 pictorially renders the aforementioned concept of a delay. Although innocuous-looking the delay gives rise to inauspicious implications.

Subsequently, what will be presented is a method which incorporates the delays in the first return map and allows for the derivation of the Monodromy matrix congruent with the delayed control laws.

6.1. First return map with one sample delay

The embodiment of the delays in the first return map can be conducted in a straightforward manner by extending the system with the addition of two states in order to describe them. Furthermore, if one acts prudently, the over-extension of the first return maps can be dispensed with which will simplify the formulation and, concomitantly, alleviated numerical computations. This can be done as follows: The state that would describe the one sample delay of $\mathbf{d}_{2,n+1}$ can be circumvented, as shown in (47), by preventing the evolution of the states for span of the period. On the other hand, this is not possible as far as $\mathbf{d}_{1,n+1}$ is concerned since the evolution of the states in this expression takes place for half a cycle and mapping them to $t = -T/2$ would instigate a

⁷ $\mathbf{P}(\mathbf{x}_n, d_1, d_2)$ and $\mathbf{P}_1(\mathbf{x}_n, d_1)$ correspond to those in Section 4.3.1.

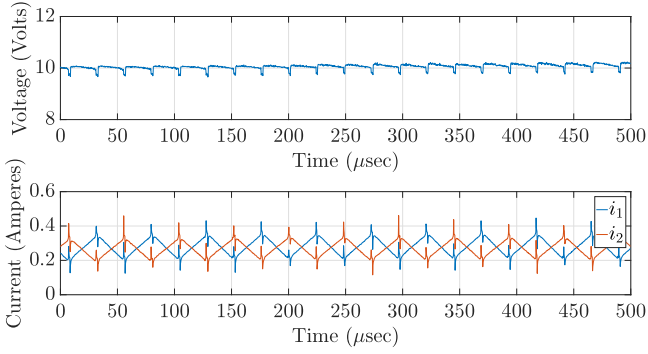
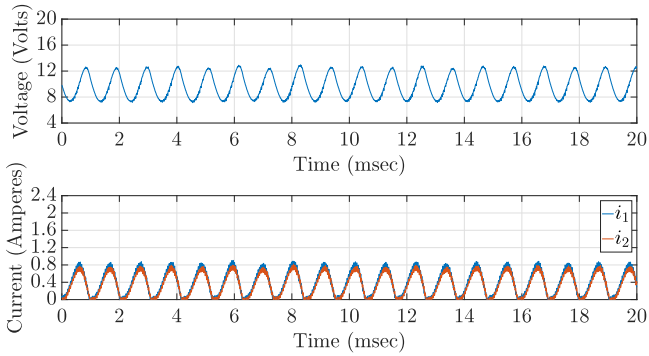
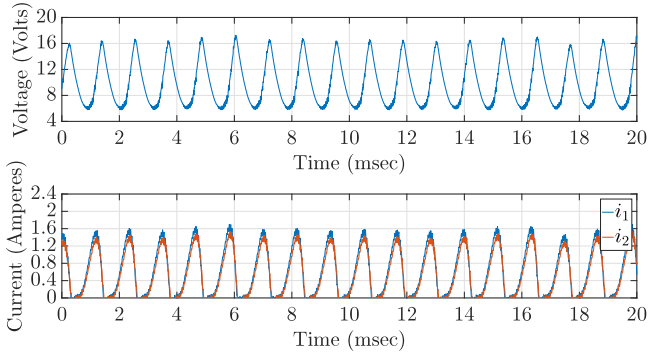


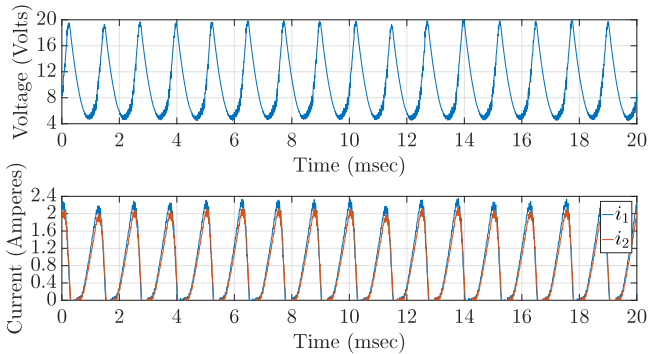
Fig. 9. Operation of the converter for $V_{ref} = 10V$ and $I_{load} = 0$. The voltage across the output capacitor is shown in the top plot and the currents through the inductors in the bottom one. The proper interleaving operation can be inferred by both the precise phase shift amongst the currents, their equal amplitude and the ripple of the output voltage.



(a) $I_{load} = 0.1$



(b) $I_{load} = 0.22$



(c) $I_{load} = 0.33$

Fig. 10. Operation of the converter for an increasing reference value of I_{load} .

dependence on past values of the duty cycles. Thus, the incorporation of the extra state that describes the delay is rendered a necessity.

In particular, the expression for \mathbf{x}_{n+1} is comprised by making use of (12) and (13) with the exception that, for $N = 1$, the duty cycle d_1 is replaced with \tilde{d}_1 that connotes the delayed duty cycle.

$$\begin{aligned} \mathbf{x}_{n+1} &= \Phi_{p1}^2 \mathbf{x}_n + \mathbf{I}_{p1}^2 \\ \mathbf{d}_{1,n+1} &= - [k_1 \quad k_2] \mathbf{C}_2 (\Phi_{p1}^1 \mathbf{x}_n + \mathbf{I}_{p1}^1) \\ &\quad - k_i T (\mathbf{x}_{4,n} - [1 \quad 0 \quad 0] (\Phi_{p1}^1 \mathbf{x}_n + \mathbf{I}_{p1}^1) + V_{ref}) \\ \tilde{d}_{1,n+1} &= d_{1,n} \\ \mathbf{d}_{2,n+1} &= - [k_1 \quad k_2] \mathbf{C}_1 \mathbf{x}_n - k_i T (\mathbf{x}_{5,n} - [1 \quad 0 \quad 0] \mathbf{x}_n + V_{ref}) \\ \mathbf{x}_{4,n+1} &= \mathbf{x}_{4,n} - [1 \quad 0 \quad 0] (\Phi_{p1}^1 \mathbf{x}_n + \mathbf{I}_{p1}^1) + V_{ref} \\ \mathbf{x}_{5,n+1} &= \mathbf{x}_{5,n} - [1 \quad 0 \quad 0] \mathbf{x}_n + V_{ref} \end{aligned} \quad (47)$$

The above case makes use of formulations and state transition pertinent to the situation where the duty cycles are above the 0.5 threshold. Nonetheless, for the other case where the duty cycles are below the threshold of 0.5 it is not a complicated task for the reader to arrive a similar map to that of (47) since the necessary tools are in disposal.

6.2. Bifurcation analysis

In order to derive the Monodromy Matrix the system (47) is linearized around the point of interest with respect to the eight state variables. The resulting expression is then evaluated around the point of interest. Table 6 was constructed to coincide with the first two entries of Table 5 in order to illustrate the impact of the delay. The eigenvalues demonstrate a Neimark–Sacker bifurcation even in the unloaded case, i.e. for $I_{load} = 0$. Consequently, as the current source sinks more current the limit cycle remains unstable.

As it was insinuated before, and corroborated by Table 6, the effects of the sample delay on the limit cycle stability are severe. Hence, a designer that engages into the construction of a converter, based on the above analysis, should be aware of the ramifications that come along. To further validate the concreteness of this assertion the next section is concerned with experimentation.

7. Experimental verification

In order to corroborate the above theoretical analysis leading to Section 6 on the consequences of digital control under interleaving operation as far limit cycle stability is concerned an experimental converter, which is pictorially outlined in Fig. 11,⁸ has been utilized. Moreover, in the majority of cases, due to physical restrictions principally stemming from micro-controller units (MCUs), the one sample delay is concomitant. Having said that the subsequent experimental results will complement Section 6.

The parameters of the converter used in the experimentation are listed in Table 1. The waveforms presented in Fig. 9 where attained in closed loop, with the state feedback gains of Section 5, and illustrate the proper operation of the converter and interleaving. However, when the electronic load is actuated to sink current the limit cycle, as it expected, bifurcates.

Fig. 10 demonstrates the operation of the converter for different values of the reference signal to the electronic load. While the reference signal I_{load} assumes increasing values the operation of the converter is exacerbated by the occurrence of a slow-scale instability. The slow-scale limit cycle instability emerges for the first time for $I_{load} = 0.1$ as shown in Fig. 10a. From this point on as I_{load} increases its effects become even more severe since the amplitude of the superimposed sinusoid is heightened. Figs. 10b and 10c can attest to the previous assertion.

⁸ Refer to the caption of Fig. 11 for a compendious description of the layout.

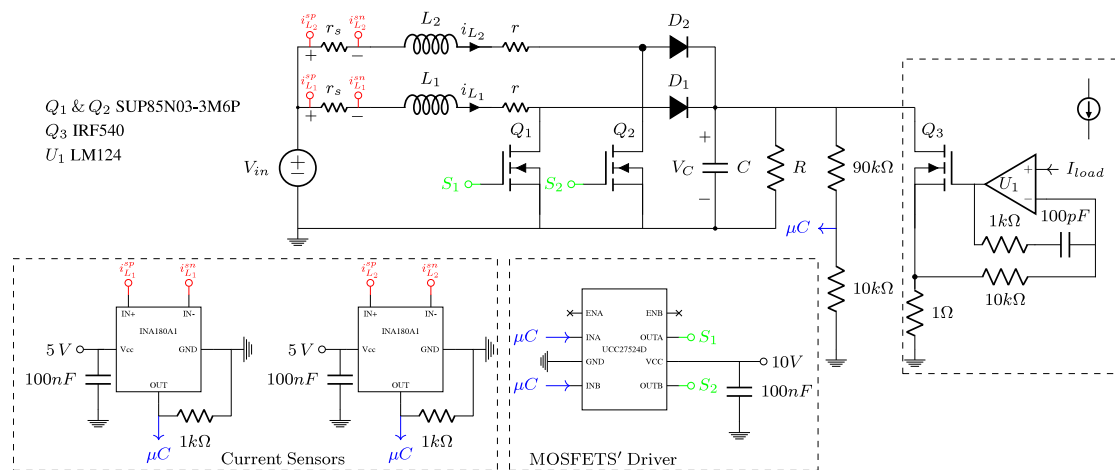


Fig. 11. Experimental layout of the 2-leg interleaved boost converter. Blue arrows diverging away from the components represent measurement signals to, and when the direction is reversed control signals from, the micro-controller which is an *ATmega256A3BU* MCU. The constant current source has been realized by an electronic load at the output of the converter. The shunt $r_s = 50$ mΩ resistors between the source and the inductors provide the input voltage to the current sensors. The rest of the pertinent components are adumbrated on the top left corner. (For interpretation of the references to colour in this figure legend, the reader is referred to the web version of this article.)

As it can be deduced the experimental results attained are in congruence with the analysis undertaken in Sections 6.1 and 6.2. Namely, the converter undergoes a slow-scale instability for very small values of the reference current in the electronic load and if increased the converter operates with voltages rising to forbidding amplitudes. The situation experimentally illustrated here further attributes to the necessity of investigated the limit cycle stability of power conversion systems.

8. Conclusions

This paper has dealt with the limit cycle stability analysis of interleaved DC–DC boost converter. The stability was investigated under static and dynamic state feedback control schemes. The reasons why these control schemes were taken into account whilst conducted the investigation is that they have been utilized by many researchers in the field due to the amenability to be cast into robust design frameworks. Although they constitute the pinnacles of state of the art control in power conversion systems their design is based on the averaged model. This gives rise to the problematic situation that the average model cannot provide full insight on the limit cycle stability of the converter.

Although the limit cycle stability of converter under digital control have been studied before little has been done for the case of interleaving. The transition might seem as an easy task the methods and analysis proposed here suggest otherwise. Several problematic situations arise when interleaving and digital control are in conjunction. This study was able to give solutions to these problems in a compendious manner by elaborating on the first return maps and the Poincaré method. Furthermore, experimentation was conducted to further validate the dynamic state feedback control scheme. It was shown that the delays that stem from digitally implementing the control laws exacerbate the stability of the limit cycle. Thus, it can be deduced that when the task of designing a control law for a converter is undertaken the limit cycle stability analysis should complement the procedure. Methods for avoiding these phenomena can be found in Aroudi et al. (2015). In addition, this is of utmost importance when someone is dealing with high power applications since the switching frequency is substantially lower and inherently gives rise to intense nonlinear phenomena.

Another contribution of this paper is that the ideas and notions that were involved in incorporating the digital control law, and especially the discrete integrator, can be further utilized to model other digital control schemes. The motivation behind this assertion is that in most cases in literature analog control schemes are utilized. They are incorporated in the systems differential equations and then discretized to arrive to the first return maps. The case where digital control laws are

employed a priori has not been meticulously addressed as opposed to this study.

Acknowledgements

The authors would like to thank Dr. Dave Atkinson and Mr. Darren Mackie for their assistance and useful advice on the development of the experimental device used in this work. The Engineering and Physical Sciences Research Council (EPSRC) of the United Kingdom is acknowledged for subsidizing this work under its doctoral programme.

Declaration of competing interest

None declared.

References

- Aizerman, M., & Gantmakher, F. (1958). On the stability of periodic motions. *Journal of Applied Mathematics and Mechanics*, 22(6), 1065–1078. [http://dx.doi.org/10.1016/0021-8928\(58\)90033-9](http://dx.doi.org/10.1016/0021-8928(58)90033-9), URL <http://www.sciencedirect.com/science/article/pii/0021892858900339>.
- Aroudi, A. E., Benadero, L., Toribio, E., & Olivar, G. (1999). Hopf bifurcation and chaos from torus breakdown in a pwm voltage-controlled DC–DC boost converter. *IEEE Transactions on Circuits and Systems I*, 46(11), 1374–1382. <http://dx.doi.org/10.1109/81.802837>.
- Aroudi, A. E., Debbat, M., & Martinez-Salamero, L. (2007). Poincaré maps modeling and local orbital stability analysis of discontinuous piecewise affine periodically driven systems. *Nonlinear Dynamics*, 50, 431–445.
- Aroudi, A. E., Iu, D. G. H. H.-C., & Hiskens, I. A. (2015). A review on stability analysis methods for switching mode power converters. *IEEE Journal on Emerging and Selected Topics in Circuits and Systems*, 5, 302–315.
- Banerjee, S., & Verghese, G. C. (2001). *Nonlinear phenomena in dc/dc converters*. Wiley-IEEE Press.
- Baushev, V. S., Zhusubaliev, Z. T., Kolokolov, Y. V., & Terekhin, I. V. (1992). Local stability of periodic solutions in sampled-data control systems. *Automation and Remote Control*, 2.
- di Bernardo, M., & Vasca, F. (2000). Discrete-time maps for the analysis of bifurcations and chaos in dc/dc converters. *IEEE Transactions on Circuits and Systems I*, 47(2), 130–143. <http://dx.doi.org/10.1109/81.828567>.
- Choi, H., Jang, M., Ciobotaru, M., & Agelidis, V. G. (2016). Performance evaluation of interleaved high-gain converter configurations. *IET Power Electronics*, 9(9), 1852–1861. <http://dx.doi.org/10.1049/iet-pel.2015.0644>.
- Cisneros, R., Pirro, M., Bergna, G., Ortega, R., Ippoliti, G., & Molinas, M. (2015). Global tracking passivity-based {PI} control of bilinear systems: application to the interleaved boost and modular multilevel converters. *Control Engineering Practice*, 43, 109–119. <http://dx.doi.org/10.1016/j.conengprac.2015.07.002>.
- Elsied, M., Oukaour, A., Chaoui, H., Gualous, H., Hassan, R., & Amin, A. (2016). Real-time implementation of four-phase interleaved DC–DC boost converter for electric vehicle power system. *Electric Power Systems Research*, 141, 210–220. <http://dx.doi.org/10.1016/j.epsr.2016.07.028>.

- Erickson, R. W., & Maksimovic, D. (2001). *Fundamentals of power electronics* (2nd ed.). Springer.
- Fadil, H. E., Giri, F., Guerrero, J., Haloua, M., & Abouloifa, A. (2011). Advanced control of interleaved boost converter for fuel cell energy generation system. *IFAC Proceedings Volumes*, 44(1), 2803–2808. <http://dx.doi.org/10.3182/20110828-6-IT-1002.03384>, 18th IFAC World Congress.
- Filippov, A. (1988). In F. Arscott (Ed.), *Differential equations with discontinuous righthand sides: Control systems* (1st ed.). Springer Netherlands.
- Gelig, A. K., & Churilov, A. (1998). *Stability and oscillations of nonlinear pulse-modulated systems* (1st ed.). Birkhäuser Basel.
- Geyer, T., Papafotiou, G., & Morari, M. (2008). Hybrid model predictive control of the step-down dc–dc converter. *IEEE Transactions on Control Systems Technology*, 16(6), 1112–1124. <http://dx.doi.org/10.1109/TCST.2008.917221>.
- Giaouris, D., Banerjee, S., Stergiopoulos, F., Papadopoulou, S., Voutetakis, S., Zahawi, B., et al. (2014). Foldings and grazings of tori in current controlled interleaved boost converters. *International Journal of Circuit Theory and Applications*, 42(10), 1080–1091. <http://dx.doi.org/10.1002/cta.1906>.
- Giaouris, D., Banerjee, S., Zahawi, B., & Pickert, V. (2008). Stability analysis of the continuous-conduction-mode boost converter via filippov's method. *IEEE Transactions on Circuits and Systems. I. Regular Papers*, 55(4), 1084–1096. <http://dx.doi.org/10.1109/TCSI.2008.916443>.
- Giaouris, D., Yfoulis, C., Voutetakis, S., & Papadopoulou, S. (2013). Stability analysis of digital state feedback controlled boost converters. In *IECON 2013 - 39th annual conference of the IEEE industrial electronics society* (pp. 8391–8396). <http://dx.doi.org/10.1109/IECON.2013.6700539>.
- Giral, R., Martinez-Salamero, L., Leyva, R., & Maixe, J. (2000). Sliding-mode control of interleaved boost converters. *IEEE Transactions on Circuits and Systems I*, 47(9), 1330–1339. <http://dx.doi.org/10.1109/81.883328>.
- Gkizas, G., Amanatidis, C., Yfoulis, C., Stergiopoulos, F., Giaouris, D., Ziogou, C., et al. (2016). State-feedback control of an interleaved dc–dc boost converter. In *2016 24th mediterranean conference on control and automation (MED)* (pp. 931–936). <http://dx.doi.org/10.1109/MED.2016.7535901>.
- Gkizas, G., Yfoulis, C., Amanatidis, C., Stergiopoulos, F., Giaouris, D., Ziogou, C., et al. (2018). Digital state-feedback control of an interleaved dc–dc boost converter with bifurcation analysis. *Control Engineering Practice*, 73, 100–111. <http://dx.doi.org/10.1016/j.conengprac.2018.01.004>, URL <http://www.sciencedirect.com/science/article/pii/S0967066118300042>.
- Guilbert, D., Gaillard, A., N'Diaye, A., & Djerdir, A. (2016). Power switch failures tolerance and remedial strategies of a 4-leg floating interleaved dc/dc boost converter for photovoltaic/fuel cell applications. *Renewable Energy*, 90, 14–27. <http://dx.doi.org/10.1016/j.renene.2015.12.054>.
- Guilbert, D., N'Diaye, A., Gaillard, A., & Djerdir, A. (2016). Fuel cell systems reliability and availability enhancement by developing a fast and efficient power switch open-circuit fault detection algorithm in interleaved dc/dc boost converter topologies. *International Journal of Hydrocarbon Engineering*, 41(34), 15505–15517. <http://dx.doi.org/10.1016/j.ijhydene.2016.01.169>.
- Jung, M., Lempidis, G., Holsch, D., & Steffen, J. (2015a). Control and optimization strategies for interleaved dc–dc converters for ev battery charging applications. In *2015 IEEE energy conversion congress and exposition (ECCE)* (pp. 6022–6028). <http://dx.doi.org/10.1109/ECCE.2015.7310504>.
- Jung, M., Lempidis, G., Holsch, D., & Steffen, J. (2015b). Optimization considerations for interleaved dc–dc converters for ev battery charging applications, in terms of partial load efficiency and power density. In *2015 17th European conference on power electronics and applications (EPE'15 ECCE-Europe)* (pp. 1–9). <http://dx.doi.org/10.1109/EPE.2015.7309164>.
- Karamanakos, P., Geyer, T., & Manias, S. (2013). Model predictive control of the interleaved dc–dc boost converter with coupled inductors. In *2013 15th European conference on power electronics and applications (EPE)* (pp. 1–10). <http://dx.doi.org/10.1109/EPE.2013.6632006>.
- König, O., Gregorčič, G., & Jakubek, S. (2013). Model predictive control of a dc–dc converter for battery emulation. *Control Engineering Practice*, 21(4), 428–440. <http://dx.doi.org/10.1016/j.conengprac.2012.12.009>.
- Michal, V. (2016). Optimal peak-efficiency control of the cmos interleaved multi-phase step-down dc–dc converter with segmented power stage. *IET Power Electronics*, 9, 2223–2228. <http://dx.doi.org/10.1049/iet-pel.2015.0814>.
- Mouli, G. R. C., Schijffelen, J. H., Bauer, P., & Zeman, M. (2017). Design and comparison of a 10-kw interleaved boost converter for pv application using si and SiC devices. *IEEE Journal of Emerging and Selected Topics in Power Electronics*, 5(2), 610–623. <http://dx.doi.org/10.1109/JESTPE.2016.2601165>.
- Pulvirenti, F., Scala, A. L., Ragonese, D., D'Souza, K., Tina, G. M., & Pennisi, S. (2013). 4-phase interleaved boost converter with ic controller for distributed photovoltaic systems. *IEEE Transactions on Circuits and Systems. I. Regular Papers*, 60(11), 3090–3102. <http://dx.doi.org/10.1109/TCSI.2013.2256235>.
- Saadi, R., Kraa, O., Ayad, M., Becherif, M., Ghodbane, H., Bahri, M., et al. (2016). Dual loop controllers using pi, sliding mode and flatness controls applied to low voltage converters for fuel cell applications. *International Journal of Hydrocarbon Engineering*, 41(42), 19154–19163. <http://dx.doi.org/10.1016/j.ijhydene.2016.08.171>.
- Salhi, B., Ahmed-Ali, T., Fadil, H. E., Magarotto, E., & Giri, F. (2013). Adaptive output feedback control of interleaved parallel boost converters. *IFAC Proceedings Volumes*, 46(11), 311–317. <http://dx.doi.org/10.3182/20130703-3-FR-4038.00063>, 11th IFAC Workshop on Adaptation and Learning in Control and Signal Processing.
- Shojaeian, H., Heydari, M., & Hasanzadeh, S. (2017). Improved interleaved high step-up converter with high efficiency for renewable energy applications. In *Power electronics, drive systems and technologies conference (PEDSTC)* (pp. 288–293). <http://dx.doi.org/10.1109/PEDSTC.2017.7910339>.
- Tseng, K.-C., & Huang, C.-C. (2014). High step-up high-efficiency interleaved converter with voltage multiplier module for renewable energy system. *IEEE Transactions on Industrial Electronics*, 61, 1311–1319. <http://dx.doi.org/10.1109/TIE.2013.2261036>.
- Wang, H., & Khaligh, A. (2015). Interleaved sepic pfc converter using coupled inductors in pev battery charging applications. In *2015 IEEE applied power electronics conference and exposition (APEC)* (pp. 586–591). <http://dx.doi.org/10.1109/APEC.2015.7104408>.
- Wu, H., Pickert, V., & Giaouris, D. (2014). Nonlinear analysis for interleaved boost converters based on monodromy matrix. In *2014 IEEE energy conversion congress and exposition (ECCE)* (pp. 2511–2516). <http://dx.doi.org/10.1109/ECCE.2014.6953735>.
- Wu, H., Pickert, V., Giaouris, D., & Ji, B. (2017). Nonlinear analysis and control of interleaved boost converter using real-time cycle to cycle variable slope compensation. *IEEE Transactions on Power Electronics*, 32(9), 7256–7270. <http://dx.doi.org/10.1109/TPEL.2016.2626119>.
- Yfoulis, C., Giaouris, D., Stergiopoulos, F., Ziogou, C., Voutetakis, S., & Papadopoulou, S. (2014). Robust constrained stabilization of a boost dc–dc converter with lyapunov-based control and piecewise-linear lyapunov functions. In *2014 European Control Conference (ECC)* (pp. 2170–2175). <http://dx.doi.org/10.1109/ECC.2014.6862531>.
- Yfoulis, C., Giaouris, D., Stergiopoulos, F., Ziogou, C., Voutetakis, S., & Papadopoulou, S. (2015). Robust constrained stabilization of boost dc–dc converters through bifurcation analysis. *Control Engineering Practice*, 35, 67–82. <http://dx.doi.org/10.1016/j.conengprac.2014.11.004>, URL <http://www.sciencedirect.com/science/article/pii/S0967066114002664>.
- Zhang, Z., Xu, C., & Liu, Y. F. (2014). A digital adaptive discontinuous current source driver for high-frequency interleaved boost PFC converters. *IEEE Transactions on Power Electronics*, 29(3), 1298–1310. <http://dx.doi.org/10.1109/TPEL.2013.2260175>.
- Zhusubaliyev, Z., A. Soukhoterina, E., & Mosekilde, E. (2001). Border-collision bifurcations and chaotic oscillations in a piecewise-smooth dynamical system. *International Journal of Bifurcation and Chaos - IJBC*, 11, 2977–3001. <http://dx.doi.org/10.1142/S0218127401003991>.
- Zhusubaliyev, Z., A. Soukhoterina, E., N. Rudakov, V., V. Kolokolov, Y., & Mosekilde, E. (2001). Bifurcations and chaotic oscillations in an automatic control relay system with hysteresis. *International Journal of Bifurcation and Chaos*, 11, 1193–1231. <http://dx.doi.org/10.1142/S0218127401002699>.
- Zhusubaliyev, Z. T., Mosekilde, E., & Yanochkina, O. O. (2011). Torus-bifurcation mechanisms in a DC/DC converter with pulsewidth-modulated control. *IEEE Transactions on Power Electronics*, 26(4), 1270–1279. <http://dx.doi.org/10.1109/TPEL.2010.2100830>.
- Zhusubaliyev, Z. T., Soukhoterina, E. A., & Mosekilde, E. (2003). Quasi-periodicity and border-collision bifurcations in a DC–dc converter with pulsewidth modulation. *IEEE Transactions on Circuits and Systems I*, 50(8), 1047–1057. <http://dx.doi.org/10.1109/TCSI.2003.815196>.